Published in final edited form as:

*Neuroscience*. 2020 November 10; 448: 272–286. doi:10.1016/j.neuroscience.2020.08.034.

# Presynaptic PRRT2 deficiency causes cerebellar dysfunction and paroxysmal kinesigenic dyskinesia

**Dylan J. Calame**[a], **Jianfeng Xiao**[b], **Mohammad Moshahid Khan**[b,c], **TJ Hollinsworth**[d], **Yi Xue**[b], **Abigail L. Person**[a], **Mark S. LeDoux**[e,f]

[a]Department of Physiology and Biophysics, University of Colorado Anschutz School of Medicine, Aurora, CO, 80045, USA

[b]Department of Neurology and Neuroscience Institute, University of Tennessee Health Science Center, Memphis, TN, 38163, USA

[c]Division of Rehabilitation Sciences, Department of Physical Therapy, College of Health Professions, University of Tennessee Health Science Center, Memphis, TN, 38163, USA

[d]Department of Ophthalmology and Hamilton Eye Institute, University of Tennessee Health Science Center, Memphis, TN, 38163, USA

[e]Department of Psychology and School of Health Studies, University of Memphis, Memphis, TN, 38152, USA

[f]Veracity Neuroscience LLC, Memphis, TN, 38157, USA

## Abstract

*PRRT2* loss-of-function mutations have been associated with familial paroxysmal kinesigenic dyskinesia (PKD), infantile convulsions and choreoathetosis, and benign familial infantile seizures. Dystonia is the foremost involuntary movement disorder manifest by patients with PKD. Using a lacZ reporter and quantitative reverse-transcriptase PCR, we mapped the temporal and spatial distribution of PRRT2 in mouse brain and showed the highest levels of expression in cerebellar cortex. Further investigation into PRRT2 localization within the cerebellar cortex revealed that *Prrt2* transcripts reside in granule cells but not Purkinje cells or interneurons within cerebellar cortex, and PRRT2 is presynaptically localized in the molecular layer. Analysis of synapses in the cerebellar molecular layer via electron microscopy showed that *Prrt2*$^{-/-}$ mice have increased numbers of docked vesicles but decreased vesicle numbers overall. In addition to impaired performance on several motor tasks, approximately 5% of *Prrt2*$^{-/-}$ mice exhibited overt PKD with clear face validity manifest as dystonia. In *Prrt2* mutants, we found reduced parallel fiber facilitation at parallel fiber-Purkinje cell synapses, reduced Purkinje cell excitability, and normal cerebellar nuclear excitability, establishing a potential mechanism by which altered cerebellar activity promotes disinhibition of the cerebellar nuclei, driving motor abnormalities in

**Correspondence:** Mark S. LeDoux (mark.ledoux@gmail.com).
**Present/permanent address:** Veracity Neuroscience LLC, 5050 Poplar Avenue, Suite 511, Memphis, TN 38157

PKD. Overall, our findings replicate, refine, and expand upon previous work with PRRT2 mouse models, contribute to understanding of paroxysmal disorders of the nervous system, and provide mechanistic insight into the role of cerebellar cortical dysfunction in dystonia.

### Keywords

*Prrt2* ; knock-out mice; dystonia; cerebellum; paroxysmal kinesigenic dyskinesia

## INTRODUCTION

The paroxysmal dyskinesias are a broad category of movement disorders characterized by the sudden onset of involuntary movements that may include dystonia, chorea, athetosis, ballism, or a combination of these (Demirkiran and Jankovic, 1995; Erro et al., 2014). The paroxysmal dyskinesias are divided into three major types: paroxysmal kinesigenic dyskinesias (PKD) precipitated by sudden movements, paroxysmal non-kinesigenic dyskinesias (PKND) triggered by alcohol or stress, and paroxysmal exertion-induced dyskinesias (PED) brought on by exertion or exercise (Demirkiran and Jankovic, 1995). Of these, PKD is the most common subtype and occurs in an autosomal dominant inheritance pattern in affected families (Bhatia, 2011; Méneret and Roze, 2018). Overall, dystonia is the foremost involuntary movement disorder manifest by patients with PKD (Méneret et al., 2012, 2013). Involuntary movements occur episodically, with attacks occurring up to 100X/day and typically lasting 5 s to 2 min (Lance, 1977; Demirkiran and Jankovic, 1995; Bhatia, 2011; Méneret and Roze, 2018). The paroxysmal dyskinesias show overlap with other paroxysmal neurological disorders (e.g., epilepsy, migraines) in terms of genetics and triggers (Méneret and Roze, 2018).

Heterozygous mutations in *PRRT2* are the most common cause of hereditary PKD (Méneret and Roze, 2018). Two hotspot *PRRT2* mutations (c.649dupC, p.R217Pfs*8; and c.649delC, p.R217Efs*12) – which likely lead to haploinsufficiency via nonsense-mediated decay of transcripts – account for up to 82% of all cases of *PRRT2*-associated PKD (Chen et al., 2011; Hedera et al., 2012; Gardiner et al., 2015; Manso-Calderón, 2019). Genetically confirmed cases have been reported in all races of people. Novel (c.776dupG, p.E260*) and hotspot (c.649dupC, p.R217Pfs*8) mutations in *PRRT2* are associated with classic PKD in individuals of African descent residing in the United States (Hedera et al., 2012). A much smaller percentage of PKD cases are associated with *PRRT2* missense mutations (Freidman et al., 2012). *PRRT2* mutations have also been causally associated with infantile convulsions and choreoathetosis, benign familial infantile seizures-2/convulsions, hemiplegic migraine, episodic ataxia, febrile seizures, and childhood-absence epilepsy disorders (Weber et al., 2004; Heron et al., 2012). Patients with biallelic *PRRT2* mutations exhibit more severe phenotypes including multiple paroxysmal disorders, learning difficulties, and prolonged episodes of ataxia (Delcourt et al., 2015).

Mouse PRRT2 shows strong homology to human *PRRT2* (Bateman et al., 2017). PRRT2 is a transmembrane protein with a relatively large intercellular N-terminus and small extracellular C-terminus (Rossi et al., 2016). Some truncating mutations may cause

mistargeting of the mutant PRRT2 protein subcellularly (Chen et al., 2011; Liu et al., 2016). PRRT2 silencing leads to decreased synaptic density (Liu et al., 2016; Valente et al., 2016), suggesting that PRRT2 has a role in synaptic formation and maintenance. Numerous protein-protein interaction studies also point to a synaptic localization of PRRT2. At the synapse, PRRT2 purportedly interacts with post-synaptic GRIA1, a component of the AMPA receptor complex (Schwenk et al., 2012; Li et al., 2015). Others have shown that PRRT2 has interactions with components of the presynaptic SNARE (soluble N-ethylmaleimide-sensitive factor attachment protein receptor) complex important for vesicle docking and release (Valente et al., 2016; Coleman et al., 2018), potentially implicating PRRT2 in both pre- and post-synaptic function. PRRT2 interactions with molecules like synaptotagmin 1/2 and SNAP-25 (Stelzl et al., 2005; Liu et al., 2016; Valente et al., 2016), suggest that it has an important role in sensing calcium to regulate synaptic fusion, as knockdown also seems to decrease synaptic transmission (Valente et al., 2016). PRRT2 interacts with Intersectin 1, an intracellular protein involved in synaptic vesicle cycling (Rossi et al., 2016). PRRT2 expression also decreases $Na^+$ current in voltage-gated $Na^+$ channels, specifically $Na_V1.2/Na_V1.6$ (Fruscione et al., 2018), indicating that it might have non-synaptic fusion roles in regulating cellular excitability.

Recent studies of *Prrt2* knockout (KO) have shown that mice exhibit mild motor abnormalities at rest, and, relative to controls, abnormal responses to seizure-inducing stimuli (Michetti et al., 2017; Tan et al., 2018). However, previous models do not clearly document paroxysmal dystonia with face and etiological validity. Previous studies have shown high levels of PRRT2 expression in the cerebellum where facilitation at parallel fiber-Purkinje cell synapses is altered, with potential abnormal pauses generated in Purkinje cells in response to high frequency stimulation. These results provide supportive evidence for cerebellar contributions to PRRT2-related dystonic behaviors but do not clearly delineate relative contributions of granule, Purkinje, and cerebellar nuclear cells. In this regard, the cerebellum has been demonstrated as a necessary locus for the generation of certain dystonias, but most dystonia-associated proteins are widely expressed in most, if not all, cerebellar cell types. For example, both caytaxin haploinsufficiency and Torsin A knockdown in the cerebellum lead to irregular bursting activity in Purkinje cells and cerebellar nuclear neurons along with manifest dystonia and expression of these dystonia phenotypes is absent without cerebellar involvement (LeDoux et al., 1998; Fremont et al., 2014).

Here, we add to, clarify, and expand upon the existing PRRT2 literature to understand how PRRT2 deficiency leads to paroxysmal dystonia (LeDoux et al., 2015). We show that *Prrt2*$^{-/-}$ mice display clear deficits in motor coordination, and, importantly, show that some of these mice display kinesigenic dystonias characteristic of human PKD, without use of unnatural experimental triggers such as pentylenetetrazol (PTZ). Using both lacZ staining and quantitative reverse-transcriptase PCR (QRT-PCR), we show that *Prrt2* is highly expressed in multiple brain regions during postnatal development, most notably in the cerebellum. Previous reports showed expression in the molecular and Purkinje cell layers of the cerebellum (Chen et al., 2011; Tan et al., 2018). Here we explicate the cell types that express PRRT2. Localization of transcript and protein demonstrates that *Prrt2* is expressed in granule cells and PRRT2 is localized to the presynaptic space in

the molecular layer of cerebellum but is not expressed in Purkinje cells, basket cells, or molecular layer interneurons. Further analysis of synapses in the cerebellar molecular layer with transmission electron microscopy (TEM) showed that *Prrt2* KO increases the number of docked vesicles but decreases reserves and total vesicle counts overall. We also show that *Prrt2* KO leads to decreased facilitation at parallel fiber-Purkinje cell synapses and changes in Purkinje cell excitability, whereas the downstream cerebellar nuclei (CbN) are unaffected, suggesting that neural dysfunction could be inherited from the circuit at the level of the Purkinje cell. Taken together, these results support the view of that cerebellar cortex is a primary locus of dysfunction in mice and humans with *Prrt2* KO, and critical to the pathophysiology of human dystonia.

## EXPERIMENTAL PROCEDURES

### Mice and genotyping

All experiments were performed in accordance with the National Institutes of Health's Guide for the Care and Use of Laboratory Animals and with approval of the Institutional Animal Care and Use Committees. All efforts were made to limit the numbers of animals used and minimize their suffering. Animals of both sexes were used in this study.

### Generation of PRRT2 KO mice

*Prrt2*$^{fl/fl}$ mice were derived from the NIH KO Mouse Project (KOMP)-Children's Hospital Oakland Research Institute, Sanger Institute, University of California Davis (CSD) KO first, promoter driven, targeted (CSD23085) ES cells. Three verified ES clones were injected into blastocysts from albino B6 donors by the Texas Institute for Genomic Medicine (TIGM). After establishment of germline transmission, the lacZ-loxP-neo cassette was removed via crossing to a FLP deleter mouse line with the mouse codon-optimized FLPo gene on the C57BL/6 background [C57BL/6N-Tg(CAG-Flpo)1Afst/Mmucd]. Floxed mice were bred to Cre-deleter mice [B6.Cg-Tg(Sox2-cre)1Amc/J] to generate targeted *Prrt2*$^{-/-}$ KO mice. *Prrt2*$^{+/-}$ mice were backcrossed to C57BL/6J mice (JAX) for at least 8 generations, and C57BL/6N (JAX) mice for at least 5 generations. Behavioral and neurophysiological experiments and qualitative assessments of involuntary movements reported herein were performed with mice on the 6J background. Mice on the 6N background were only utilized for qualitative assessments of involuntary movements.

### Behavioral testing

Mice were subjected to a battery of motor and behavioral examinations including open-field activity, rotarod, vertical rope climbing, raised-beam task, grip strength, gait analysis (DigiGait™), dominance tube, and cross-maze test. Except for the righting reflex, all testing was performed in adult mice (3 mo.) over a period of 5 days. Mice were returned to their home cages for a period of at least 30 min prior to individual tests. For the righting reflex, postnatal mice were placed in the supine position and then released. The time required for all four limbs to contact the tabletop was measured for three trials.

For the open-field activity assay, mice were placed in activity monitors (MED Associates, Inc., Georgia, VT, USA) for 10-min sessions. The activity monitors measured 27 × 27 cm,

with 16 infrared photocell beams equally spaced in the x and y axes of the horizontal plane, 1 cm from the floor of the chambers. An additional array of 16 photocells was situated 5 cm above the floor to track rearing. All tests were conducted in the dark. One hour prior to testing, cages were moved from the housing racks to a quiet anteroom adjacent to the testing room. Following this period of habituation, animals were removed from their home cage, immediately placed in the center of the open field and allowed to freely explore the apparatus for a test interval of 10 min. Animals were scored for a number of behaviors including total distance traveled (cm). The data recorded during testing was scored in post-session analyses using Activity Monitor 5.1 (Med Associates). The testing apparatus was cleaned with a 15% ethanol solution and allowed to air dry between mice. Mice were given 1 trial at the same time daily for 3 consecutive days. Median values of activity parameters were used for statistical comparisons.

Mice were acclimated to a Rotamex-5 rotarod (Columbus Instruments, Columbus, OH, USA) rotating at 5 rpm for 5 min on the day prior to data acquisition. On the following day, mice were exposed to a 30 s acclimation period at 4 rpm followed by an acceleration of 4 rpm every 30 s to a target of 40 rpm at 5 min. Mice were given 3 trials at the same time each day for 5 consecutive days. Median values were used for statistical comparisons.

Mice were acclimated to a vertical, 40-cm long, 10-mm thick nylon rope prior to testing. The bottom of the rope was suspended 15 cm above a padded base and the top entered a darkened escape box. Three trials with a 5-min inter-trial interval were completed for each mouse. Median times were used for statistical analysis of vertical rope climbing.

For the raised-beam task, mice were acclimated to an 80-cm long, 20-mm wide beam elevated 50 cm above a padded base. A 60 W lamp at the start served as an aversive stimulus, whereas the opposite end of the beam entered a darkened escape box. Transversal time and number of slips were measured as mice traversed the beam. After initial testing with a 20-mm diameter square beam, mice were given follow-up tests using supplementary round (12-mm and 9-mm diameter) and square (12-mm and 9-mm diameter) beams. All testing was performed in triplicate and median values were used for subsequent statistical analyses.

To measure grip strength, mice were held by the scruff of the neck with one hand and the base of the tail with the other hand. Mice were then free to grasp a metal grid attached to a force meter (Columbus Instruments, Columbus, OH, USA) as they were moved along the axis of the grid. Maximal strength (g) with which mice pulled the grid was measured in triplicate trials with a minimal inter-trial interval of 5 min. Median values were used for subsequent statistical analyses.

The DigiGait™imaging system consists of a motorized treadmill with a digital camera positioned below a transparent belt (Mouse Specifics Inc., Boston, MA). For each mouse, the location and timing of each paw contact on the belt was automatically recorded at a belt speed of 20 cm/s for 5 s. A minimum of 800 video frames collected at 160 frames/s was digitized and gait parameters were calculated by the accompanying software. Three trials

with 30 min inter-trial intervals were completed for each mouse. Median values were used for statistical analysis.

The cross-maze analysis testing apparatus consisted of 4 radial arms, each 25 cm-long, and a camera along with ANY-maze software (Stoelting Co., Wood Dale, IL, USA). Mice were placed into the apparatus for 5 min and entries into each arm were recorded sequentially using an ABCD format with each letter representing an individual arm of the maze. Alternation was counted if mice went into radial arms sequentially (% alternations = 100 × total alternations / [total entries − 3]).

The dominance tube test was used for identifying a general abnormality in social interaction through the measurement of aggression. Mice of different genotypes were released into opposite ends of a dark, narrow tube (30-cm long). Mice interacted in tube and the more dominant or aggressive mouse forced its opponent out of the tube. When one animal had all four paws out of the tube, it was declared the loser while the animal remaining inside the tube was the winner, ending the match. The number of wins was reported as a percentage of the total number of matches. The match was deemed a draw when both mice remained in the tube >120 s.

Mice were weighed weekly. Video recordings and righting reflex assays were performed prior to weaning. Mice were observed for the presence of spontaneous and stimulus-induced (handling, trunk and limb displacement with a microspatula, snout tap, and tail pinch) abnormal movements daily from Postnatal Day 1 (P1) through P30 and then 3X weekly through 6 months of age. Qualitative assessments of videotaped recordings were performed by an experienced investigator (MSL) blinded to genotype.

### Expression of *Prrt2* transcript

Relative levels of mouse *Prrt2* mRNA were determined in 6 brain regions (cerebral cortex, cerebellum, hippocampus, striatum, thalamus, and midbrain), cervical spinal cord, and liver harvested from 3 adult male mice of each genotype ($Prrt2^{+/+}$, $Prrt2^{+/-}$, and $Prrt2^{-/-}$). TaqManbased QRT-PCR was performed using two primer pairs and probes (Table S1) with a LightCycler® 480 System (Roche, Indianapolis, IN, USA). Mouse β-actin and hypoxanthineguanine phosphoribosyltransferase (HGPRT) were used as endogenous controls.

### RNAScope *in-situ* hybridization

RNAScope Fluorescent Multiplex Assay kit (Cat. No. 320850; Advanced Cell Diagnostics) was used to examine the cellular localization of *Prrt2*. Mice were rapidly anesthetized with pentobarbital (100 mg/kg, IP) and transcardially perfused with 4% paraformaldehyde in 0.1 M sodium phosphate buffer (PB) (pH 7.4). Brains were removed and post-fixed in the same solution overnight and cryo-protected with 30% sucrose in PB at 4 °C. Cerebella were sectioned on a cryostat at 10 μm thickness and incubated in boiling antigen retrieval solution at 99–100°C for 5–10 min. Slides were washed in water two times for 1 min each and were dipped in 100% ethanol and air dried. Slides were then incubated with protease IV for 20 min at 40°C. After protease treatment, slides were incubated with RNAScope target probes for 2 hrs at 40°C, followed by signal amplification per the manufacturer's

instructions. Target probes (mouse-*Prrt2* [Cat. No. 502661, NM_001102563.1] and mouse-*Calb1-C2* [Cat No. 428431, NM_009788.4]) along with negative control probe (Cat No. 320871) were used for transcript localization. DAPI was added to label nuclei. Images were captured with a Zeiss 710 laser scanning confocal microscope.

## Expression of PRRT2

Western blots were performed using two brains from each of four genotypes ($Prrt2^{+/+}$, $Prrt2^{fl/fl}$, $Prrt2^{+/-}$, and $Prrt2^{-/-}$). Cerebellum tissue was dissected out of each mouse brain and lysed with ice-cold RIPA lysis buffer (ThermoFisher Scientific, Waltham, MA, USA) containing Halt™ protease and phosphatase inhibitor cocktail (Thermo Fisher Scientific) using a Teflon glass homogenizer. Lysed samples were microcentrifuged for 15 min at 14000 rpm and the supernatants were collected. Samples containing equal amounts of protein were separated by electrophoresis on 4–12% Bis-Tris gels and transferred to PVDF membrane membranes using a BioRad (Berkeley, CA, USA) wet transfer system. After blocking, membranes were incubated overnight at 4°C with primary rabbit anti-PRRT2 antibody (HPA014447–100UL, MilliporeSigma, St Louis, MO, USA), followed by goat anti-rabbit HRP-conjugated secondary antibody (Jackson ImmunoResearch Laboratories, West Grove, PA, USA) for 1 hr with constant rocking at room temperature. Proteins recognized by the antibody were visualized by enhanced chemiluminescence (Amersham, Pittsburgh, PA, USA). Blots were stripped and reprobed for α-tubulin (Abcam) as a loading control. Bands intensity was measured by densitometry and quantified using NIH-Image J software.

## X-Gal staining

X-Gal staining was performed with a LacZ Detection kit for tissues (catalog #rep-lz-t Version #04J05-SV from InvitroGen, San Diego, CA USA). Groups of mice harboring the *Prrt2* lacZ-loxP-neo cassette at Postnatal Days 7 (P7), 15 (P15), 30 (P30), and 90 (P90) were transcardially fixed with 4% paraformaldehyde in 0.1 M PB pH 7.4 with 2mM $MgCl_2$. Embryos were fixed in same fixative overnight. Brains were dissected and immerged into cryoprotective solution (30% sucrose in 0.1 M PB with 2 mM $MgCl_2$) overnight. Coronal and sagittal cryosections (40 μm) were obtained and rinsed in PBS pH 7.4 with 2 mM $MgCl_2$. Floating sections were then incubated with X-Gal staining solution with 6 mM potassium ferricyanide, 6 mM potassium ferrocyanide, 2 mM $MgCl_2$, 0.02% IGEPAL®, 0.01% Na-deoxycholate, and 1 mg/ml X-Gal Solution in PBS overnight at 37 °C. Sections were then rinsed with PBS, mounted and counterstained with Nuclear Fast Red Solution (H-3402, Vector Laboratories, Burlingame, CA, USA), dehydrated, and coverslipped. All brains are stained/processed simultaneously.

## PRRT2 immunohistochemistry

Animals were overdosed with pentobarbital sodium solution (100 mg/kg, IP) prior to transcardial perfusion with ice-cold saline and perfusion fixed with 4% paraformaldehyde in 0.1 M PB, pH 7.4. Brains were dehydrated and embedded in 56 °C paraffin and 5 μm sections were collected onto SuperFrost®-Plus glass slides (Fisher Scientific, Pittsburgh, PA, USA).

For immunohistochemical detection of PRRT2, paraffin sections were first treated with antigen retrieval solution (Citrate-based H-3300, Vector Laboratories) and rinsed with distilled water and PBS. Cryostat and paraffin sections were incubated in quenching buffer, 10% methanol and 1% $H_2O_2$ in 0.02 M phosphate buffered saline (PBS) for 5 min. Sections were then blocked and permeabilized in PBS containing 2% nonfat dry milk and 0.3% Triton X-100 (Sigma-Aldrich). Sections were then incubated overnight with rabbit anti-PRRT2 antibody (HPA014447; MilliporeSigma, Burlington, MA, USA) diluted 1:200 in PBS with 3% normal serum (Jackson ImmunoResearch Laboratories, West Grove, PA, USA) and 0.1% Triton X-100. Sections were then incubated with biotinylated anti-rabbit antibody diluted in PBS with 2% normal serum and 0.1% Triton X-100 for 2 hrs, ABC complex (Vector Laboratories) for 2 hrs, then reacted with DAB solution for visualization. Between each step, slides were thoroughly rinsed with PBS. After the final rinse, slides were dehydrated and coverslipped with Permount (Fisher Scientific).

### Fluorescent immunohistochemistry and colocalization analysis

Mice were anesthetized and subsequently fixed using cardiac perfusion of 4% paraformaldehyde in PB, pH 7.4. Brains were quickly removed, and cerebella were dissected out. Tissues were dehydrated with 30 min incubations in a graded ethanol series (50%, 70%, 85%, 95%, and 100%) then cleared via a 30-min incubation in graded xylene (2:1, 1:1, and 1:2 ethanol:xylene), and two rinses of 100% xylene. Tissues were then infiltrated with paraffin using a graded paraffin series with 30-min incubations in 2:1, 1:1, and 1:2 xylene:paraffin and 2 subsequent 1-hr incubations in 100% paraffin. Paraffin-embedded tissue was sectioned at 8 μm. Sections were deparaffinized and rehydrated, treated for heat-mediated antigen retrieval by boiling in sodium citrate buffer (10 mM sodium citrate, 0.05% Tween-20) for 1 hr, washed in PBS twice and subsequently blocked in 10% goat serum/5% BSA/0.5% TritonX-100 in PBS for 30 min at RT. Sections were subsequently incubated in 1:500 anti-PRRT2 (MilliporeSigma), anti-vGlut1 (Catalog #: 135 316; Synaptic Systems, Goettingen, Germany), and anti-GluR1 (Catalog #: SAB5201086, MilliporeSigma) antibodies overnight at 4°C. The following day, slides were rinsed in PBS, 3 × 5 min, and incubated in secondary antibody (1:500 dilutions of goat anti-rabbit IgG conjugated to AlexaFluor488, goat anti-chicken IgY conjugated to AlexaFluor555, or goat anti-mouse IgG conjugated to AlexaFluor647, Thermo-Fischer) and finally stained for DAPI (Thermo-Fischer) to demarcate nuclei. Slides were then washed in PBS 4 × 5 minutes and mounted using Prolong Diamond mountant (Thermo-Fischer). Slides were imaged on a Zeiss 710 LSM at 200X and 630X magnifications and colocalization analysis was performed using Imaris software (Bitplane, Concord, MA, USA). Spots were assigned to the labeling based on peak mean intensities and colocalization was analyzed using a threshold of 0.5 μm.

### TEM analysis of vesicles docked at synapses

Mice were anesthetized and subsequently transcardially perfused with 4% paraformaldehyde and 2% glutaraldehyde in 0.1 M sodium cacodylate buffer, pH 7.4. Brains were removed and whole cerebella collected and immersion-fixated overnight at 4 °C in the same solution. Tissue was then sliced longitudinally and washed in 0.1 M sodium cacodylate buffer, pH 7.4, 3 × 20 min, and post-fixed in 1% osmium tetroxide for 1 hr at room temperature. After osmication, tissue was washed in 0.1 M sodium cacodylate buffer, pH 7.4, for 20 min and

rinsed in distilled water 2 × 20 min before being dehydrated with 30 min incubations in a graded ethanol series and then a transitional solvent of 1:1 ethanol:propylene oxide for 30 min and finally twice in 100% propylene oxide for 30 min each. Tissue was then infiltrated overnight in 1:1 propylene oxide:Embed812 resin. The following day, tissue was further infiltrated in 100% Embed812 resin 3 × 2 hrs. Post-infiltration, tissue was flat embedded in Embed812 resin and baked for 48 hrs at 65 °C. Once embedded, the tissue was sectioned at 65 nm through the surface of the cerebellum. Sections were stained using Uranyless stain (Electron Microscopy Sciences) for 30 min and lead citrate (Electron Microscopy Sciences) for 2 min. Sections were imaged on a JEOL 2000EX Electron Microscope and vesicular numbers and distances to the synaptic cleft were measured using ImageJ by an investigator blinded to genotype.

## Cerebellar slice electrophysiology

P7-P24 mice were anesthetized with isoflurane, transcardially perfused, and decapitated. Cerebella were removed and sliced into 300 μm coronal sections using a Leica VT1000S Vibratome in the same solution used for incubation heated to 37 °C. Cerebellar slices were then incubated at 37 °C for 1 hr in oxygenated ACSF containing: 123.75 mM NaCl, 3.5 mM KCl, 26 mM $NaHCO_3$, 1.25 mM $NaH_2PO_4$, 1.5 mM $CaCl_2$, 1 mM $MgCl_2$, and 10 mM glucose. Following incubation, slices were transferred to a recording chamber perfused with oxygenated ACSF heated to 35–37 °C. Whole-cell recordings of Purkinje cells were made using 2–4 MΩ pulled borosilicate glass pipettes filled with a K-gluconate based internal stock solution containing: 130 mM K-gluconate, 2 mM Na-gluconate, 2 mM $MgCl_2$, 1 mM EGTA, 10 mM HEPES, 4 mM sucrose, 14 mM TRIS creatine phosphate, 4 mM Mg-ATP, and 0.3 mM Mg-GTP. Parallel fiber axons were stimulated electrically at 20 Hz, 0.1 ms pulse width, for 500 ms using a twisted steel electrode placed at least 50 μm from the Purkinje cell being recorded from. Recordings were made in current clamp and voltage clamp mode, amplified with a Multiclamp 700B amplifier, digitized at 20 kHz with a Digidata 1440A digitizer, and acquired with pClamp acquisition software. Data were analyzed in IGOR Pro (Wavemetrics) with the Neuromatic package (ThinkRandom). Only Purkinje cells that fired at 0 and 100 pA injected current, indicative of healthy neurons, were used in analysis. Investigators were blinded to mouse genotypes during electrophysiological recordings and analysis, with genotyping performed postmortem.

## Statistics

We used blinded random tests to analyze differences between groups. We used ordinary one-way analysis of variance (ANOVA) with Tukey's multiple comparison test to analyze differences among *Prrt2*$^{+/+}$, *Prrt2*$^{+/-}$, and *Prrt2*$^{-/-}$ mice and two-way repeated measures ANOVA with Tukey's multiple comparison test to analyze differences among genotypes across time or conditions. In direct comparisons, unpaired t-tests (assumes normal distribution) and Mann-Whitney (no assumption) tests were used.

# RESULTS

## *Prrt2* expression in the developing mouse brain

To characterize the temporal and spatial distribution of *Prrt2* expression in the developing mouse brain, we generated $Prrt2^{fl/fl}$ mice using KO first, promoter driven, targeted ES cells which harbor a lacZ-loxP-neo cassette (Fig. S1). X-Gal staining was used to define the temporal and spatial distribution of *Prrt2* expression in mice expressing the *Prrt2*-lacZ reporter (Fig. 1A). In comparison to other dystonia-associated genes such as *Sgce*, *Tor1a* and *Thap1* (Xiao and LeDoux, 2003; Xiao et al., 2004; Zhao et al., 2013), *Prrt2* expression patterns were unique. The highest expression levels were seen in the cerebellar cortex, within the granule cell layer, and in the cerebellar nuclei at multiple developmental stages (Fig. 1B). Strong expression was also seen in the thalamus and entorhinal cortex with moderate expression in the brainstem and posterior hippocampus (Fig. 1C, S2). Immunohistochemistry with a rabbit polyclonal antibody against PRRT2 showed strong staining in the molecular layer of cerebellar cortex (Fig. 1D).

Quantification of *Prrt2* transcript expression in six brain regions, cervical spinal cord, and liver using QRT-PCR closely matched observations with X-Gal staining (Fig. 1E). *Prrt2* expression was the highest in cerebellum at all stages of development. Liver expression was absent at all ages, confirming that expression is largely restricted to the nervous system. Interestingly, *Prrt2* expression in all brain and spinal structures peaks at P30 then declines thereafter, suggesting an important role for development processes in the pathobiology of PRRT2-associated neurological disorders.

## Generation of *Prrt2* KO mouse lines

To assess the functional and behavioral relevance of *Prrt2* expression in mouse brain, the lacZ-loxP-neo cassette was removed via crossing to Flp-deleter mice and *Prrt2* simple KO mice were subsequently generated via crosses with Cre-deleter mice (Fig. S1). Western blot analysis of PRRT2 expression demonstrated absence of PRRT2 in $Prrt2^{-/-}$ mice with approximately 50% reduction in heterozygotes (Fig. 2A). Semi-quantitative analysis of Western blot data showed that the loxP sites in our PKD model system are functional and the wild-type (WT) *Prrt2* allele does not exhibit significant up-regulation in $Prrt2^{+/-}$ mice (Fig. 2B). Immunohistochemistry further demonstrates the clear absence of PRRT2 in the cerebellar cortex of $Prrt2^{-/-}$ mice (Fig. 2C).

## *Prrt2* KO mice exhibit motor abnormalities and kinesigenic dystonia

In human PKD, loss-of-function *PRRT2* mutations can cause profound paroxysmal dysfunction of the nervous system with manifestations ranging from ataxia and dystonia to seizures. To assess the behavioral relevance of *Prrt2* KO, physical and behavioral effects were examined with blinded assessments of open-field behavior and a battery of sensorimotor tests. $Prrt2^{-/-}$ and $Prrt2^{+/-}$ mice of both sexes were underweight relative to their $Prrt2^{+/+}$ littermates throughout development and into adulthood (n= 10 $Prrt2^{+/+}$, 22 $Prrt2^{+/-}$, 10 $Prrt2^{-/-}$; one-way ANOVA of male weights at week 12; $F_{(2,19)} = 26.3$, $P = 3.4 \times 10^{-6}$; one-way ANOVA of female weights at week 12; $F_{(2,17)} = 13.3$, $P = 3.3 \times 10^{-4}$; Fig. 3A). Differences in the righting reflex were absent across days between genotypes, but

*post hoc* testing revealed transient differences between *Prrt2*$^{-/-}$ and *Prrt2*$^{+/-}$ mice relative to *Prrt2*$^{+/+}$ littermates that emerged at P10-P14 and disappeared in adulthood (two-way repeated measures ANOVA with Tukey's multiple comparison test; *Prrt2*$^{+/+}$ vs. *Prrt2*$^{-/-}$, adjusted *P* value at P10 = 0.035, P12 = 0.0037, P14 = $1.1 \times 10^{-6}$; *Prrt2*$^{+/+}$ vs. *Prrt2*$^{+/-}$, adjusted *P* value at P12 = 0.0089, P14 = $7.0 \times 10^{-5}$; *Prrt2*$^{+/-}$ vs. *Prrt2*$^{-/-}$, adjusted *P* value at P14 = $1.4 \times 10^{-4}$; Fig. 3B). *Prrt2* KO significantly impaired rope climbing (one-way ANOVA with Tukey's multiple comparison test; $F_{(2,39)} = 12.6$, $P = 5.9 \times 10^{-5}$; Fig. 3C), raised-beam walking (one-way ANOVA with Tukey's multiple comparison test; $F_{(2,39)} = 7.3$, $P = 0.0021$; Fig. 3D), and decreased performance across days on a rotarod assay (two-way repeated measures ANOVA; genotype: $F_{(2, 39)} = 5.5$, $P = 0.0079$; Fig. 3E). *Prrt2*$^{-/-}$ mice also showed quantitative locomotor and activity abnormalities. Open-field behavioral monitoring showed increased activity in *Prrt2*$^{-/-}$ mice relative to *Prrt2*$^{+/+}$ littermates. KO mice also had a higher stride frequency and shorter stride length (Tables S2 and S3), possibly attributable to smaller body size. These results are compatible with previous reports of gait abnormalities in *Prrt2*$^{-/-}$ mice (Michetti et al., 2017). Interestingly, in virtually all motor assays, we show that the degree of motor dysfunction was determined by whether animals had loss of a single copy or both copies of *Prrt2* (*Prrt2*$^{+/-}$ vs. *Prrt2*$^{-/-}$), indicating a direct relationship between PRRT2 levels and degree of neurological dysfunction.

Humans with heterozygous and biallelic *PRRT2* mutations exhibit kinesigenic dystonias following sudden rapid movements in response to environmental stimuli (Demirkiran and Jankovic, 1995; Bhatia, 2011; Méneret and Roze, 2018). Previous studies have shown that *Prrt2* KO mice exhibit sound-induced audiogenic seizures without progression to overt myoclonic or tonic-clonic seizures and differentially-characterized PTZ-evoked seizures comparted to WT controls (Michetti et al., 2017; Tan et al., 2018), leaving open the question of whether *Prrt2* KO mice actually exhibit kinesigenic dystonia. To assess whether *Prrt2* KO mice exhibited kinesigenic dystonias like humans, we subjected mice to a battery of sudden perturbations. By P7, and peaking at P11 to P13, approximately 5 to 10% of *Prrt2*$^{-/-}$ mice and 3 to 5% of *Prrt2*$^{+/-}$ mice exhibited variable combinations of truncal, hindlimb, and forelimb dystonias ranging from quite subtle to overt (Videos 1 - 3). Like human phenotypes, dystonic posturing lasted less than 2 min. In addition, some *Prrt2*$^{+/-}$ mice and many *Prrt2*$^{-/-}$ mice exhibited periods of apparent behavioral arrests and semi-rhythmic truncal movements during this developmental window (Video 4). Smaller numbers of mice displayed paroxysmal gait dysfunction characterized by dystonic extension of the hindlimbs with elevation of the caudal trunk (Video 5). Electroencephalography was not performed as part of these studies. After P20, paroxysmal dystonia was milder, less frequent, and progressively more difficult to detect. Qualitative assessments did not expose a clear effect of genetic background (6J vs. 6N). Combined, these results indicate that PRRT2 deficiency causes motor impairments and can closely emulate the clinical features of human PKD. Of note, mice were only observed for < 15 min daily or every other day in their home cage or plexiglass holding chamber. We did not monitor for the presence of abnormal movements at night or within the context of environmental enrichment.

### *Prrt2* is expressed in granule cells and localized presynaptically in the cerebellar molecular layer

High levels of cerebellar *Prrt2* expression point to potential cerebellar roles in the motor manifestations of *Prrt2* KO in our mouse model and human PKD, more generally. However, there exist conflicting reports about the localization and the role of PRRT2 in neurons and cerebellar circuits (Chen et al., 2011; Schwenk et al., 2012; Li et al., 2015; Valente et al., 2016; Coleman et al., 2018). To characterize PRRT2 localization in the cerebellar circuit on a cellular level, we investigated expression patterns of both RNA transcripts and PRRT2 proteins. *In-situ* hybridization targeting *Prrt2* transcripts showed RNA expression localized exclusively to the granule cell layer in cerebellar cortex (Fig. 4A). Transcripts were notably absent in $Prrt2^{-/-}$ mice. Immunofluorescent staining of the PRRT2 protein showed expression in the granule cell layer and molecular layer of cerebellar cortex. No colocalization of PRRT2 with calbindin was seen, indicating PRRT2 is not expressed in Purkinje cells (Fig. 4B). Spot colocalization analysis of PRRT2 with pre- and post-synaptic proteins, vGlut1 and GluR1, respectively, was used to determine the synaptic location of PRRT2 (Fig. 4E). PRRT2 label was highly colocalized with vGlut1, whereas we saw virtually no PRRT2 colocalization with GluR1 (n = 3 animals each; unpaired t-test; PRRT2-vGlut1 vs. PRRT2-GluR1: $P = 0.0012$) confirming that expression in cerebellar cortex is presynaptic.

### *Prrt2* KO increases vesicle docking and decreases reserve vesicles in the cerebellar cortex

We next sought to understand the role of PRRT2 at the presynapse in the molecular layer of cerebellar cortex. PRRT2 has been shown to interact with a collection of presynaptic proteins in the SNARE complex critical for vesicle docking (Valente et al., 2016; Coleman et al., 2018). To investigate whether KO affects vesicles in the molecular layer of cerebellar cortex, we used TEM to quantify synaptic docking in $Prrt2^{+/+}$ and $Prrt2^{-/-}$ cerebellar cortex (Fig. 5A, B). $Prrt2^{-/-}$ mice had, on average, only 35.7± 6.91 (mean ± SEM) total vesicles/synapse compared to 44.3 ± 3.53 in $Prr2^{+/+}$ littermates (n = 37 synapses each; Mann-Whitney test; $P = 0.0004$; Fig. 5C), On the other hand, $Prrt2^{-/-}$ mice had an increased number of docked vesicles in the same slices (Mann-Whitney test; $P = 6.9 \times 10^{-8}$; Fig. 5E). Interestingly, this disparity can be, at least partly explained by fewer reserve vesicles in $Prrt2^{-/-}$ mice (Mann-Whitney test; $P = 9.4 \times 10^{-6}$; Fig. 5D). Changes in vesicle numbers and docking at this synapse suggest the possibility of electrophysiological consequences downstream in Purkinje cells and nuclear cell cerebellar outputs.

### *Prrt2* KO decreases facilitation at parallel fiber-Purkinje cell synapses and alters the firing properties of Purkinje cells

Previous reports have shown an increased facilitation profile after many stimuli at parallel fiber-Purkinje cell synapses with variable responses early in stimulation (Michetti et al., 2017; Tan et al., 2018). Given the highly similar dystonic profile that our KO mouse line shares with humans, we sought to test the effect of *Prrt2* KO on synaptic transmission at parallel fiber to Purkinje cell synapses. We electrically stimulated parallel fibers in the molecular layer at 20 Hz while recording EPSCs in Purkinje cells and, surprisingly, found that facilitation seen in Purkinje cells across trains of stimulation was clearly decreased

in *Prrt2*$^{-/-}$ mice (Fig. 6A). Normalized EPSC amplitudes measured at a −70 mV holding potential for both *Prrt2*$^{+/-}$ and *Prrt2*$^{-/-}$ groups were significantly diminished at all successive stimuli, with *Prrt2*$^{-/-}$ slices showing EPSC amplitudes only 1.42 ± 0.11 times baseline (mean ± SEM) at the final stimulus, relative to 2.09 ± 0.19 seen in *Prrt2*$^{+/+}$ controls (n= *Prrt2*$^{+/+}$: 10 cells, 8 mice; *Prrt2*$^{+/-}$: 13 cells, 8 mice; *Prrt2*$^{-/-}$: 9 cells, 6 mice; two-way repeated measures ANOVA with Tukey's multiple comparison test; genotype: $F_{(2,29)} = 8.4$, $P = 0.0013$; Fig. 6B).

Next, to assess differences in cerebellar function that might be inherited from parallel fiber-Purkinje cell synaptic dysfunction in *Prrt2*$^{-/-}$ animals, we performed whole-cell patch-clamp experiments in cerebellar Purkinje cells and CbN cells in acute cerebellar slices (Fig. 6C). When assessing how Purkinje cells responded to injected current steps, we found significantly different firing rates between genotypes. *Prrt2*$^{-/-}$ Purkinje cells showed consistently diminished excitability in response to current injection relative to *Prrt2*$^{+/+}$ and *Prrt2*$^{+/-}$ cells (*Prrt2*$^{+/+}$: 17 cells, 13 mice; *Prrt2*$^{+/-}$: 24 cells, 13 mice; *Prrt2*$^{-/-}$: 11 cells, 6 mice; two-way repeated measures ANOVA with Tukey's multiple comparison test; genotype: $F_{(2,50)} = 5.5$, $P = 0.0068$; Fig. 6D). Interestingly, even with 0 injected current, *Prrt2*$^{-/-}$ Purkinje cells fired at a much lower frequency of 25.4 ± 7.7 Hz (mean ± SEM) relative to 88.8 ± 17.3 Hz seen in *Prrt2*$^{+/+}$. Similar recordings in the CbN showed no significant differences in the firing rate in response to injected current steps (*Prrt2*$^{+/+}$: 11 cells, 7 mice; *Prrt2*$^{+/-}$: 12 cells, 5 mice; *Prrt2*$^{-/-}$: 7 cells, 5 mice; two-way repeated measures ANOVA with Tukey's multiple comparison test; genotype: $F_{(2,27)} = 0.77$, $P = 0.47$; Fig. 6E). These results suggest that PRRT2 deficiency may, indirectly, alter the excitability properties of Purkinje cells and this altered firing profile could be fed through the otherwise unaffected cerebellar nuclei to generate motor abnormalities.

## DISCUSSION

Using a *Prrt2* null mouse model of PKD, we were able to recapitulate clinical features of human PKD, most notably paroxysmal dystonia, and extend published experimental evidence related to the causal role of PRRT2 deficiency in mouse motor deficits. We confirm that the dominant locus of *Prrt2* expression is the presynapse of parallel fibers within the molecular layer of cerebellar cortex. *Prrt2* is not expressed at readily detectable levels in molecular layer interneurons or Purkinje cells. We also show that the absence of PRRT2 causes abnormal distribution of synaptic vesicles in the presynapse with increases in the number of docked vesicles, while decreasing vesicle reserves. These subcellular abnormalities in PRRT2-deficient mice are accompanied by decreased facilitation at the parallel fiber-Purkinje cell synapse. Lastly, we show that PRRT2 deficiency reduces Purkinje cell excitability, perhaps due to the developmental effects of pathological granule cell input, which could lead to abnormal disinhibition of the cerebellar nuclei, which we show have normal excitability despite expressing *Prrt2.* This circuit deficit predicts pathological output from the cerebellum contributing to the motor phenotype seen in PKD.

## Behavioral ramifications of PRRT2 KO

The observation that *Prrt2* KO mice exhibit hallmark clinical features of PKD, particularly kinesigenic appendicular and truncal dystonia, supports the close resemblance of our model to *PRRT2*-associated disease in humans. Moreover, our finding that only a small percentage of mice exhibited paroxysmal involuntary movements during daily observation (LeDoux et al., 2015) is compatible with the human phenotype with the mean maximum frequency of attacks being 11/day (Ebrahimi-Fakhari et al., 2015). In contrast, previous reports of motor deficits in *Prrt2* KO models have focused on behavioral phenotypes driven by triggers such as hyperthermia, induced seizures, and optogenetic stimulation (Michetti et al., 2017, Tan et al., 2018). Previous studies also report rare nondescript "paroxysms" at 5 weeks to 8 months of age (Robertson et al., 2019), or flurothyl-induced myoclonic jerks (Pan et al., 2020).

In addition to paroxysmal involuntary movements characteristic of human PKD, we also identified gait abnormalities and other motor defects that seem to be shared with other reports of *Prrt2* KO models (Michetti et al., 2017, Tan et al., 2018). Like the autosomal dominant pattern of disease inheritance in humans, we found that $Prrt2^{+/-}$ heterozygotes display quantitative motor impairments. Consistent with this observation, we saw no compensatory upregulation of *Prrt* expression in $Prrt2^{+/-}$ mice that would serve to rescue the motor phenotype. Another notable similarity between our mouse model of PKD and human disease is that the involuntary movement disorder was transient, disappearing in adulthood. Human PKD often ameliorates with aging, in some cases with complete remission (Bruno et al., 2004). Parallel timelines of disease appearance and remission suggest that there are similar time courses of *Prrt2* expression – possibly as a result of shared epigenetic patterning – in mice and humans, further validating the mouse as a suitable model to study *PRRT2*-related PKD.

## Timescale of PRRT2 expression and its implications

To isolate the locus of *Prrt2* influence on the brain we used X-Gal staining and showed that *Prrt2* is expressed in multiple brain regions – most extensively in the cerebellar granule cell layer – and tightly developmentally regulated consistent with previous reports (Michetti et al., 2017). We did not see expression outside of the developing nervous system. QRT-PCR corroborated this pattern and showed that *Prrt2* has clear temporal regulation – peaking at P30, somewhat parallel to the window of the PKD-associated motor phenotype – suggesting that it may have unique roles in neurodevelopment. As PRRT2 has been implicated in synaptic formation and maintenance (Liu et al., 2016; Valente et al., 2016), it is important to note that *Prrt2* expression largely matches the time course of synaptogenesis in rodents (Berry and Bradley, 1976; Micheva and Beaulieu, 1996; Li et al., 2010). This possible implication of PRRT2 in early-life brain processes could explain why PKD symptoms are most manifest early in life, with many cases of remission in adulthood.

## Effects of PRRT2 KO on synaptic function

Using both analysis of RNA transcripts and PRRT2 proteins, we were able to show that, in the cerebellar cortex, *Prrt2* expression is limited to the granule cell layer, and PRRT2 protein is highly expressed in the molecular layer of cortex. Previous studies have suggested that PRRT2 is also expressed in the Purkinje cell layer and that it interacts with AMPA receptor

components (Schwenk et al., 2012; Li et al., 2015). Our results show that PRRT2 does not colocalize with Purkinje cell marker calbindin, and a careful analysis of PRRT2 localization in the molecular layer showed that PRRT2 colocalizes with presynaptic proteins. Further analysis of PRRT2 localization using *in-situ* hybridization confirmed that *Prrt2* expression is only seen in granule cells, and not molecular layer interneurons in the cerebellar cortex, or Purkinje cells. In agreement with this presynaptic localization of PRRT2, TEM analysis of these synapses show that PRRT2 KO affects vesicle localization. Specifically, PRRT2 seems to act as a negative regulator of vesicle docking. These data fit nicely with the proposed interaction of PRRT2 with SNAP-25 and synaptotagmin 1/2 in the SNARE complex (Valente et al., 2016; Coleman et al., 2018) and reports of an increased number of docked vesicles in the hippocampus and cerebellum with PRRT2 loss (Valente et al., 2016, Tan et al., 2018). Importantly, here we show that while the number of docked vesicles were higher in *Prrt2*$^{-/-}$ animals, we observed a decrease in the number of total and reserve vesicles in the cerebellar molecular layer. Our results contrast to what has been observed in the hippocampus where total vesicle number is unchanged with *Prrt2* knockdown (Valente et al., 2016).

WT parallel fiber-Purkinje cell synapses show robust short-term facilitation (Perkel et al., 1990, Regehr and Atluri, 1995; Atluri and Regehr, 1996; Isope and Barbour, 2002; Valera et al., 2012). We speculate that the changes in synaptic vesicles we detailed could drive differences between *Prrt2*$^{-/-}$ and *Prrt2*$^{+/+}$ synaptic transmission. Previous reports indicated that PRRT2 plays an essential role in regulating synchronous release, specifically in the $Ca^{2+}$ dependent transition from priming to fusion (Valente et al., 2016). We found that *Prrt2* KO profoundly decreased short-term facilitation at the parallel fiber-Purkinje cell synapse, suggesting that without PRRT2 to negatively regulate synaptic docking, normal facilitation is lost. Similar experiments examining parallel fiber physiology in *Prrt2* transgenic mice showed increased facilitation following many stimuli (Michetti et al., 2017; Tan et al., 2018) with similar findings in the hippocampus (Valente et al., 2019). Because we did not extend analyses beyond 10 stimuli, it is difficult to know whether we would have seen this same increased facilitation profile after many stimuli. Nevertheless, the deficit we observed is consistent with reduced drive of Purkinje neurons, a circuit-level effect that could disinhibit cerebellar output. Potential experimental conditions that could underlie this discrepancy are the use of physiological ACSF calcium concentrations (1.5 mM) in the present study (Silver and Erecinska, 1990; Rancz et al., 2007) rather than the 2 mM used in previous work (Michetti et al., 2017). Calcium concentration is likely significant given that PRRT2 has a proposed role in calcium sensing at the presynapse (Valente et al., 2016; Coleman et al., 2018). Small changes in calcium could profoundly affect the electrophysiological consequences of PRRT2 KO at these synapses.

Although WT Purkinje cells do not appear to express *Prrt2*, Purkinje cells in *Prrt2*$^{-/-}$ slices had lower baseline firing rates and reduced excitability, with attenuated responses to injected current. Since measurements were made in the absence of synaptic blockers, our findings indicate that *Prrt2*$^{-/-}$ Purkinje cells in relatively intact circuits have altered firing properties at different levels of depolarization. This suggests a non-cell autonomous change in cerebellar physiology where Purkinje cells inherit dysfunctional firing characteristics from altered parallel fiber-Purkinje cell synapses. Other studies have also shown that PRRT2

KO effects on parallel fiber-Purkinje cell synapses can lead to aberrant firing in Purkinje cells following high frequency stimulation of parallel fibers (Tan et al., 2018). Here, however, we have shown that even without high-frequency stimulation of synaptic input, Purkinje cell firing is altered in *Prrt2*$^{-/-}$ mice at multiple levels of depolarization. In contrast, cells in the CbN do not have differences in basal firing rate or responses to injected current, suggesting that aberrant activity of Purkinje neurons could be relayed downstream to induce motor deficits.

## Clinical correlates of PRRT2 pathology

Because Purkinje cells are inhibitory onto tonically-active CbN neurons, decreased Purkinje cell activity observed in PRRT2 KOs would result in higher tone in the CbN projections exiting the cerebellum, potentially explaining the efficacy of low-dose carbamazepine and phenytoin – sodium channel blockers that decrease neuronal excitability – on paroxysmal dystonia (Demirkiran and Jankovic, 1995; Chou et al., 2014; Mink, 2015). Alternatively, bursts of Purkinje cell activity due to paroxysmal release of glutamate at parallel fiber synapses could drive transient bursting activity in the CbN as described in the dystonic rat and a mouse model of rapid-onset dystonia-parkinsonism (LeDoux et al., 1998; Fremont et al., 2014). Others have suggested that the palliative effects of these drugs point to a channelopathy underlying the pathology of PKD (Margari et al., 2005; Pan et al., 2019), and interaction of PRRT2 with $Na_V$ in mice give weight to this model (Fruciione et al., 2018). We have shown that PRRT2 KO changes excitability in cells not expressing PRRT2 (i.e., Purkinje cells), indicating that, in addition to potential channelopathy effects of *Prrt2* KO, cellular activity is altered without PRRT2 absence causing changes in cellular channels. This observation possibly explains why PKD responds to a broad spectrum of anticonvulsants in addition to carbamazepine and phenytoin including phenobarbital, levetiracetam, gabapentin, valproic acid, oxcarbazepine, lamotrigine, and topiramate (Goodenough et al., 1978; Chudnow et al., 1997; Überall and Wenzel, 2000; Chattergee et al., 2002; Tsao, 2004; Huang et al., 2005; Erro et al., 2014; Mink, 2015)– which act on a wide range of channels, possibly compensating for changes in neuronal excitability resulting from PRRT2 loss. PRRT2 inactivation has been shown to have effects on the excitability of neurons in hippocampal slices and primary cell cultures (Valente et al., 2019) indicating a complex role of PRRT2 in generating excitability throughout the brain at the level of both synapses and ion channels.

## Summary

We have shown that absence of PRRT2 leads to hallmark clinical characteristics of PKD in mice, particularly kinesigenic dystonia characteristic of human disease. In mice, we isolated the major locus of *Prrt2* expression to the synapses of parallel fibers in the molecular layer of cerebellar cortex, where using TEM we saw an increased number of docked vesicles, with fewer vesicles overall. Electrophysiological analysis showed that PRRT2-deficient mice had decreased short-term facilitation at parallel fiber-Purkinje cell synapses and altered Purkinje cell excitability, without similar dysfunction of CbN cells, implicating cerebellar cortex as a causal agent in the motor phenotypes seen in PKD. Future validation of our model will require replication of our behavioral and neurophysiological findings after conditional deletion of PRRT2 in cerebellar granule cells.

## Supplementary Material

Refer to Web version on PubMed Central for supplementary material.

## Acknowledgements:

Mice were generated while Dr. LeDoux was a faculty member at the University of Tennessee Health Science Center

**Funding:**

This work was supported by grants from the NIH (NS094965), Dystonia Medical Research Foundation, and Benign Essential Blepharospasm to MSL.

## REFERENCES

Atluri PP, Regehr WG (1996) Determinants of the time course of facilitation at the granule cell to Purkinje cell synapse. J Neurosci 16:5661–5671. [PubMed: 8795622]

Bateman A et al. (2017) UniProt: The universal protein knowledgebase. Nucleic Acids Res 45:D158–D169. [PubMed: 27899622]

Berry M, Bradley P (1976) The growth of the dendritic trees of Purkinje cells in the cerebellum of the rat. Brain Res 112:1–35. [PubMed: 947479]

Bhatia KP (2011) Paroxysmal dyskinesias. Mov Disord 26:1157–1165. [PubMed: 21626559]

Bruno MK, Hallett M, Gwinn-Hardy K, Sorensen B, Considine E, Tucker S, Lynch DR, Mathews KD, Swoboda KJ, et al. (2004) Clinical evaluation of idiopathic paroxysmal kinesigenic dyskinesia: new diagnostic criteria. Neurology 63:2280–2287. [PubMed: 15623687]

Chattergee A, Louis E, Frucht S (2002) Levetiracetam in the treatment of paroxysmal kinesiogenic choreoathetosis. Mov Disord 17:614–615. [PubMed: 12112221]

Chen WJ, Lin Y, Xiong ZQ, Wei W, Ni W, Tan GH, Guo SL, He J, et al. (2011) Exome sequencing identifies truncating mutations in PRRT2 that cause paroxysmal kinesigenic dyskinesia. Nat Genet 43:1252–1255. [PubMed: 22101681]

Chou IC, Lin SS, Lin De W, Wang CH, Chang YT, Tsai FJ, Tsai CH (2014) Successful control with carbamazepine of family with paroxysmal kinesigenic dyskinesia of PRRT2 mutation. Biomed 4:51–53.

Chudnow RS, Mimbela RA, Owen DB, Roach ES (1997) Gabapentin for familial paroxysmal dystonic choreoathetosis Multiorgan dysfunction and disseminated intravascular coagulation in children receiving lamotrigine and valproic acid. Neurology 49:1441–1442. [PubMed: 9371936]

Coleman J, Jouannot O, Ramakrishnan SK, Zanetti MN, Wang J, Salpietro V, Houlden H, Rothman JE, et al. (2018) PRRT2 regulates synaptic fusion by directly modulating SNARE complex assembly. Cell Rep 22:820–831. [PubMed: 29346777]

Delcourt M, Riant F, Mancini J, Milh M, Navarro V, Roze E, Humbertclaude V, Korff C, et al. (2015) Severe phenotypic spectrum of biallelic mutations in PRRT2 gene. J Neurol Neurosurg Psychiatry 86:782–785. [PubMed: 25595153]

Demirkiran M, Jankovic J (1995) Paroxysmal dyskinesias: clinical features and classification. Ann Neurol 38:571–579. [PubMed: 7574453]

Ebrahimi-Fakhari D, Saffari A, Westenberger A, Klein C (2015) The evolving spectrum of PRRT2associated paroxysmal diseases. Brain 138:3476–3495. [PubMed: 26598493]

Erro R, Sheerin UM, Bhatia KP (2014) Paroxysmal dyskinesias revisited: a review of 500 genetically proven cases and a new classification. Mov Disord 29:1108–1116. [PubMed: 24963779]

Freidman J, Olvera J, Silhavy J, Gabriel S, Gleeson J (2012) Mild paroxysmal kinesigenic dyskinesia caused by PRRT2 missense mutation with reduced penetrance. Neurology 79:946–948. [PubMed: 22895590]

Fremont R, Calderon DP, Maleki S, Khodakhah K (2014) Abnormal high-frequency burst firing of cerebellar neurons in rapid-onset dystonia-parkinsonism. J Neurosci 34:11723–11732.

Fruscione F, Valente P, Sterlini B, Romei A, Baldassari S, Fadda M, Prestigio C, Giansante G, et al. (2018) PRRT2 controls neuronal excitability by negatively modulating $Na^+$ channel 1.2/1.6 activity. Brain 141:1000–1016. [PubMed: 29554219]

Gardiner AR, Jaffer F, Dale RC, Labrum R, Erro R, Meyer E, Xiromerisiou G, Stamelou M, et al. (2015) The clinical and genetic heterogeneity of paroxysmal dyskinesias. Brain 138:3567–3580. [PubMed: 26598494]

Goodenough DJ, Fariello RG, Annis BL, Chun RWM (1978) Familial and acquired paroxysmal dyskinesias: a proposed classification with delineation of clinical features. Arch Neurol 35:827–831. [PubMed: 718486]

Hedera P, Xiao J, Puschmann A, Momčilović D, Wu SW, LeDoux MS (2012) Novel PRRT2 mutation in an African-American family with paroxysmal kinesigenic dyskinesia. BMC Neurol 12:1. [PubMed: 22289169]

Heron SE, Grinton BE, Kivity S, Afawi Z, Zuberi SM, Hughes JN, Pridmore C, Hodgson BL, et al. (2012) PRRT2 mutations cause benign familial infantile epilepsy and infantile convulsions with choreoathetosis syndrome. Am J Hum Genet 90:152–160. [PubMed: 22243967]

Huang YG, Chen YC, Du F, Li R, Xu GL, Jiang W, Huang J (2005) Topiramate therapy for paroxysmal kinesigenic choreoathetosis. Mov Disord 20:75–77. [PubMed: 15390133]

Isope P, Barbour B (2002) Properties of unitary granule cell→Purkinje cell synapses in adult rat cerebellar slices. J Neurosci 22:9668–9678. [PubMed: 12427822]

Lance JW (1977) Familial paroxysmal dystonic choreoathetosis and its differentiation from related syndromes. Ann Neurol 2:285–293. [PubMed: 617268]

LeDoux MS, Hurst DC, Lorden JF (1998) Single-unit activity of cerebellar nuclear cells in the awake genetically dystonic rat. Neuroscience 86:533–545. [PubMed: 9881867]

LeDoux MS, Xiao J, Xue J, Marquez-Lona EM, Vemula SR (2015) PRRT2 deficiency causes paroxysmal dystonia in mice. Program No. 583.02. 2015 Neuroscience Meeting Planner. Washington, DC: Society for Neuroscience, 2018. Online.

Li M, Cui Z, Niu Y, Liu B, Fan W, Yu D, Deng J (2010) Synaptogenesis in the developing mouse visual cortex. Brain Res Bull 81:107–113. [PubMed: 19751806]

Li M, Niu F, Zhu X, Wu X, Shen N, Peng X, Liu Y (2015) PRRT2 mutant leads to dysfunction of glutamate signaling. Int J Mol Sci 16:9134–9151. [PubMed: 25915028]

Liu YT, Nian FS, Chou WJ, Tai CY, Kwan SY, Chen C, Kuo PW, Lin PH, et al. (2016) PRRT2 mutations lead to neuronal dysfunction and neurodevelopmental defects. Oncotarget 7:39184–39196.

Manso-Calderón R (2019) The spectrum of paroxysmal dyskinesias. Future Neurol 14:FNL26.

Margari L, Presicci A, Ventura P, Margari F, Perniola T (2005) Channelopathy: hypothesis of a common pathophysiologic mechanism in different forms of paroxysmal dyskinesia. Pediatr Neurol 32:229–235. [PubMed: 15797178]

Méneret A et al. (2012) PRRT2 mutations: A major cause of paroxysmal kinesigenic dyskinesia in the European population. Neurology 79:170–174. [PubMed: 22744660]

Méneret A, Gaudebout C, Riant F, Vidailhet M, Depienne C, Roze E (2013) PRRT2 mutations and paroxysmal disorders. Eur J Neurol 20:872–878. [PubMed: 23398397]

Méneret A, Roze E (2018) Paroxysmal movement disorders: an update. Rev Neurol (Paris) 172:433–445..

Michetti C, Castroflorio E, Marchionni I, Forte N, Sterlini B, Binda F, Fruscione F, Baldelli P, et al. (2017) The PRRT2 knockout mouse recapitulates the neurological diseases associated with PRRT2 mutations. Neurobiol Dis 99:66–83. [PubMed: 28007585]

Micheva KD, Beaulieu C (1996) Quantitative aspects of synaptogenesis in the rat barrel field cortex with special reference to GABA circuitry. J Comp Neurol 373:340–354. [PubMed: 8889932]

Mink JW (2015) Treatment of raroxysmal dyskinesias in children. Curr Treat Options Neurol 17:1–6.

Pan G, Zhang L, Zhou S (2019) Clinical features of patients with paroxysmal kinesigenic dyskinesia, mutation screening of PRRT2 and the effects of morning draughts of oxcarbazepine. BMC Pediatr 19:1–7. [PubMed: 30606158]

Pan Y, Liu Q, Zhang J, Yang Y, Tian Y, Zeng J, Yin P, Mei L, et al. (2020) PRRT2 frameshift mutation reduces its mRNA stability resulting loss of function in paroxysmal kinesigenic dyskinesia. Biochem Biophys Res Commun 522:553–559. [PubMed: 31785815]

Perkel DJ, Hestrin S, Nicoll RA (1990) Excitatory synaptic currents in Purkinje cells. Proc Biol Sci 241:116–121. [PubMed: 1978337]

Rancz EA, Ishikawa T, Duguid I, Chadderton P, Mahon S, Häusser M (2007) High-fidelity transmission of sensory information by single cerebellar mossy fibre boutons. Nature 450:1245–1248. [PubMed: 18097412]

Regehr WG, Atluri PP (1995) Calcium transients in cerebellar granule cell presynaptic terminals. Biophys J 68:2156–2170. [PubMed: 7612860]

Robertson L, Featherby T, Howell S, Hughes J, Thomas P (2019) Paroxysmal and cognitive phenotypes in *Prrt2* mutant mice. Genes Brain Behav 18:e12566.

Rossi P, Bruno S, Castroflorio E, Marte A, Onofri F, Valtorta F, Maragliano L, Corradi A, et al. (2016) A novel topology of proline-rich transmembrane protein 2 (PRRT2): hints for an intracellular function at the synapse. J Biol Chem 291:6111–6123. [PubMed: 26797119]

Schwenk J, Harmel N, Brechet A, Zolles G, Berkefeld H, Müller CS, Bildl W, Baehrens D, et al. (2012) High-resolution proteomics unravel architecture and molecular diversity of native AMPA receptor complexes. Neuron 74:621–633. [PubMed: 22632720]

Silver I, Erecinska M (1990) Intracellular and extracellular Changes of [Ca2+] in hypoxia and ischemia in ratbBrain in vivo. J Gen Physiol 95:837–866. [PubMed: 2163431]

Stelzl U, Worm U, Lalowski M, Haenig C, Brembeck FH, Goehler H, Stroedicke M, Zenkner M, et al. (2005) A human protein-protein interaction network: A resource for annotating the proteome. Cell 122:957–968. [PubMed: 16169070]

Tan GH, Liu YY, Wang L, Kui L, Zhang ZQ, Li HF, Yang ZF, Yang Li et al. (2018) PRRT2 deficiency induces paroxysmal kinesigenic dyskinesia by regulating synaptic transmission in cerebellum. Cell Res 28:90–110. [PubMed: 29056747]

Tsao C-Y (2004) Effective treatment with oxcarbazepine in paroxysmal kinesigenic choreoathetosis. J Child Neurol 19:300–301. [PubMed: 15163097]

Überall MA, Wenzel D (2000) Effectiveness of lamotrigine in children with paroxysmal kinesigenic choreoathetosis. Dev Med Child Neurol 42:699–700. [PubMed: 11085299]

Valente P, Castroflorio E, Rossi P, Fadda M, Sterlini B, Cervigni RI, Prestigio C, Giovedi S, et al. (2016) PRRT2 Is a key component of the Ca2+-dependent neurotransmitter release machinery. Cell Rep 15:117–131. [PubMed: 27052163]

Valente P, Romei A, Fadda M, Sterlini B, Lonardoni D, Forte N, Fruscione F, Castroflorio E, et al. (2019) Constitutive inactivation of the PRRT2 gene alters short-term synaptic plasticity and promotes network hyperexcitability in hippocampal neurons. Cereb Cortex 29:2010–2033. [PubMed: 29912316]

Valera AM, Doussau F, Poulain B, Barbour B, Isope P (2012) Adaptation of granule cell to Purkinje cell synapses to high-frequency transmission. J Neurosci 32:3267–3280. [PubMed: 22378898]

Weber YG, Berger A, Bebek N, Maier S, Karafyllakes S, Meyer N, Fukuyama Y, Halbach A, et al. (2004) Benign familial infantile convulsions: linkage to chromosome 16p12-q12 in 14 families. Epilepsia 45:601–609. [PubMed: 15144424]

Xiao J, Gong S, Zhao Y, LeDoux MS (2004) Developmental expression of rat torsinA transcript and protein. Dev Brain Res 152:47–60. [PubMed: 15283994]

Xiao J, LeDoux MS (2003) Cloning, developmental regulation and neural localization of rat ε-sarcoglycan. Mol Brain Res 119:132–143. [PubMed: 14625080]

Zhao Y, Xiao J, Gong S, Clara JA, LeDoux MS (2013) Neural expression of the transcription factor THAP1 during development in rat. Neuroscience 231:282–295. [PubMed: 23219941]

## Highlights

- *Prrt2*$^{-/-}$ mice exhibit paroxysmal dystonia with face validity.
- *Prrt2* transcripts reside in granule cells but not Purkinje cells or interneurons within cerebellar cortex.
- In the cerebellar molecular layer, *Prrt2*$^{-/-}$ mice have increased numbers of docked vesicles but decreased total vesicles.
- In *Prrt2*$^{-/-}$ mice, we found reduced parallel fiber facilitation at parallel fiber-Purkinje cell synapses.

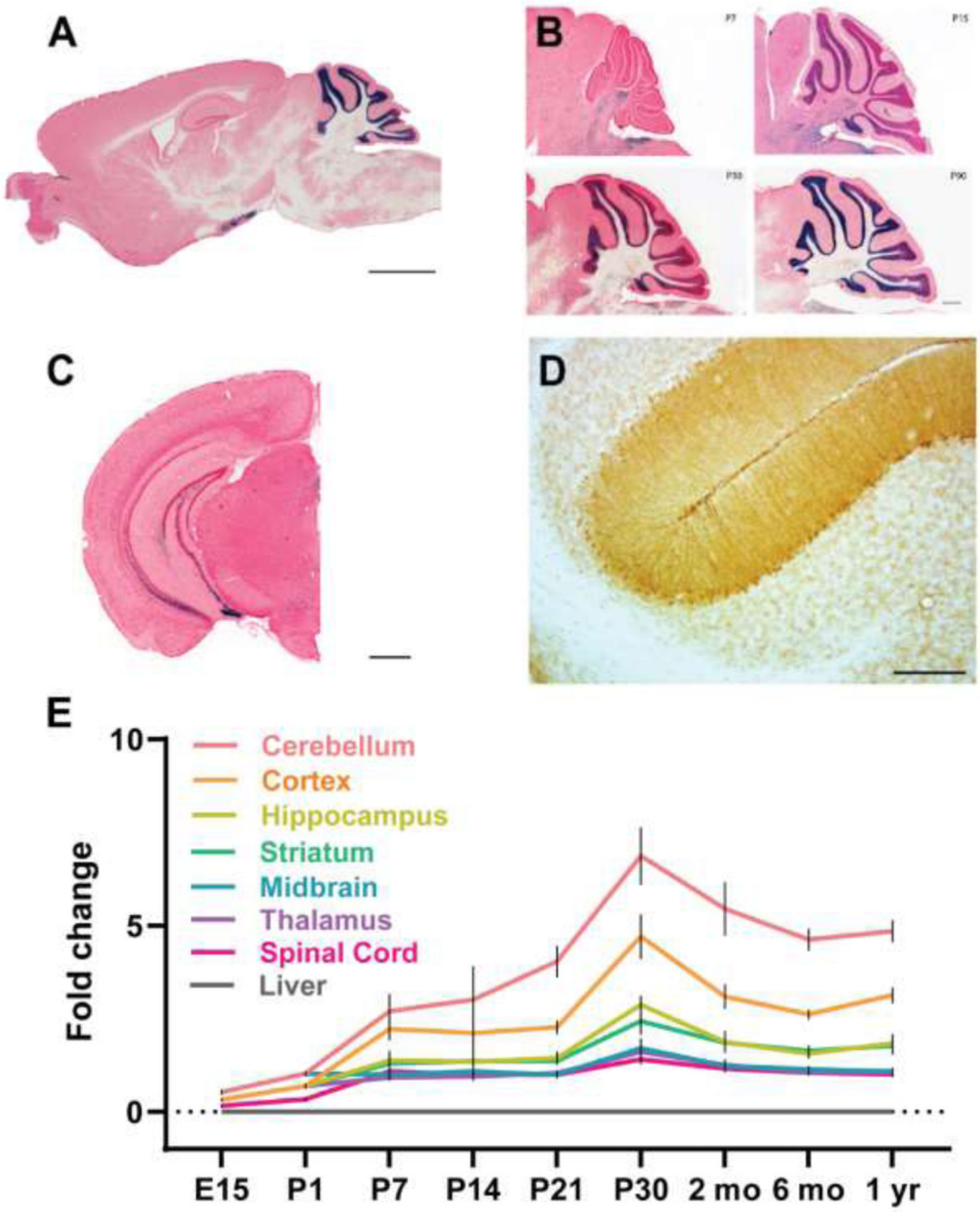


**Figure 1. *Prrt2* expression throughout the developing mouse brain and spinal cord.**

**A.** X-Gal staining of parasagittal brain section. **B.** *Prrt2* expression levels in the cerebellum at P7, P15, P30, and P90. **C.** Moderate *Prrt2* expression is seen in the hippocampus. **D.** Immunohistochemistry of cerebellar cortex suggests that PRRT2 protein is mainly located in the molecular layer. **E.** Developmental expression of *Prrt2* in mouse relative to E15 frontal cortex (n=6; mean ± SD). Dissection of all brain regions readily identifiable in older mice (midbrain, frontal cortex, striatum, cerebellum, thalamus, hippocampus, and spinal cord) was not possible at E15 and P1. Scale bar: A = 2mm, B = 500mm, C = 200mm, D = 100mm.

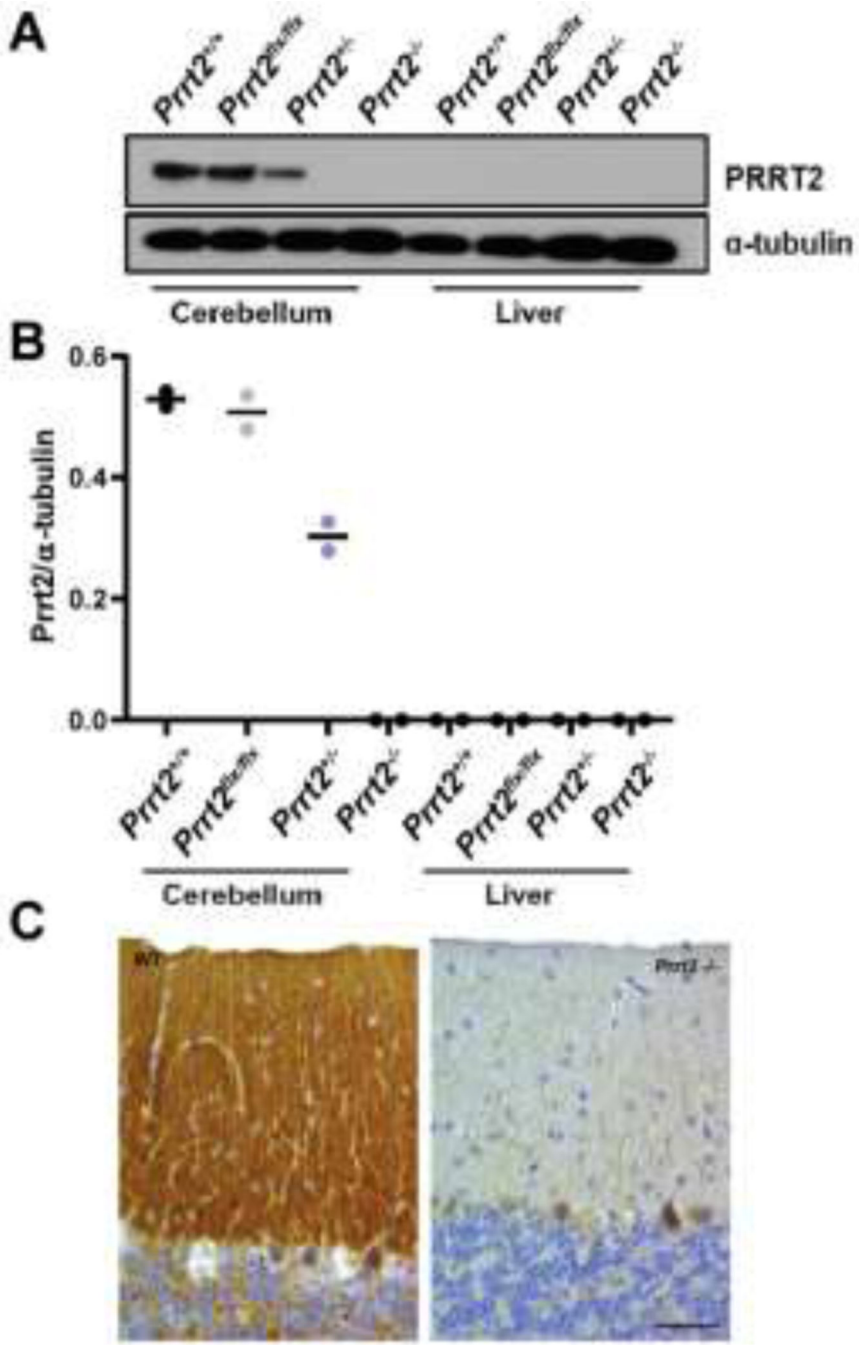


**Figure 2. Characterization of a *Prrt2* knockout model**

**A.** Left: Western blot of PRRT2 in cerebellum of *Prrt2*$^{+/+}$, *Prrt2*$^{fl/fl}$, *Prrt2*$^{+/-}$, and *Prrt2*$^{-/-}$ mice (top), with α-tubulin positive control. Right: Western blot of liver tissues in the same groups shows no expression of PRRT2. **B.** Semi-quantitative analysis of Western blot data (n=2; line = mean). **C.** PRRT2 immunohistochemistry in cerebellar cortex with rabbit anti-PRRT2 antibody. Scale bar = 50 μm.

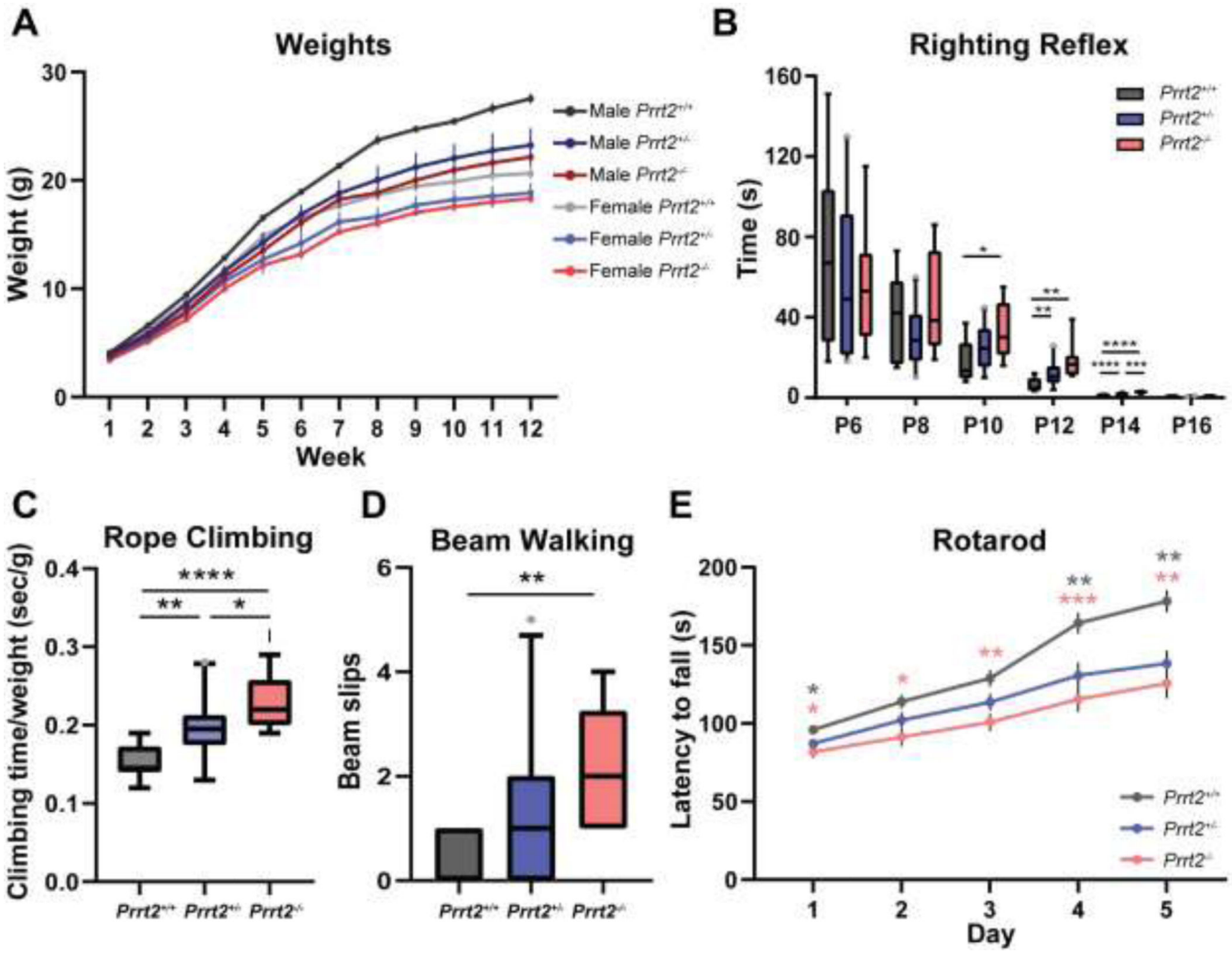


**Figure 3. Phenotypic and motor deficiencies in *Prrt2* knockout mice.**

**A.** Weights of *Prrt2*$^{+/+}$, *Prrt2*$^{+/-}$, and *Prrt2*$^{-/-}$ mice by sex (mean ± SD). **B.** Righting reflex impairments in *Prrt2*$^{+/-}$ and *Prrt2*$^{-/-}$ mice relative to their WT littermates emerge at P10 and disappear by P16 (two-way repeated measures ANOVA with Tukey's multiple comparison test; genotype: $F_{(2,39)} = 0.65$, $P = 0.53$; asterisks indicate significance in Tukey's multiple comparison test; box shows 25$^{th}$ to 75$^{th}$ percentiles, inner line is median, whiskers show 5$^{th}$ and 95$^{th}$ percentiles). **C.** Increased rope climbing time in *Prrt2*$^{+/-}$ and *Prrt2*$^{-/-}$ mice normalized for weight (one-way ANOVA with Tukey's multiple comparison test; $F_{(2,39)} = 12.6$, $P = 5.9 \times 10^{-5}$; asterisks indicate significance in Tukey's multiple comparison test; box shows 25$^{th}$ to 75$^{th}$ percentiles, inner line is median, whiskers show 5$^{th}$ and 95$^{th}$ percentiles) **D.** *Prrt2*$^{+/-}$ and *Prrt2*$^{-/-}$ mice showed decreased motor coordination on a round 9mm raised-beam task (one-way ANOVA with Tukey's multiple comparison test; $F_{(2,39)} = 7.3$, $P = 0.0021$; asterisks indicate significance in Tukey's multiple comparison test; box shows 25$^{th}$ to 75$^{th}$ percentiles, inner line is median, whiskers show 5$^{th}$ and 95$^{th}$ percentiles) **E.** Performance on the rotarod task was impaired in *Prrt2*$^{+/-}$ and *Prrt2*$^{-/-}$ mice across multiple days (two-way repeated measures ANOVA with Tukey's multiple comparison test;

genotype: $F_{(2,39)} = 5.5$, $P = 0.0079$; asterisks indicate significance in Tukey's multiple comparison test; pink asterisks = *Prrt2*$^{+/+}$ vs *Prrt2*$^{-/-}$, grey asterisks = *Prrt2*$^{+/+}$ vs *Prrt2*$^{+/-}$; mean ± SEM). * = $P<0.5$, ** = $P<0.01$; *** = $P<0.001$; **** = $P<0.0001$.

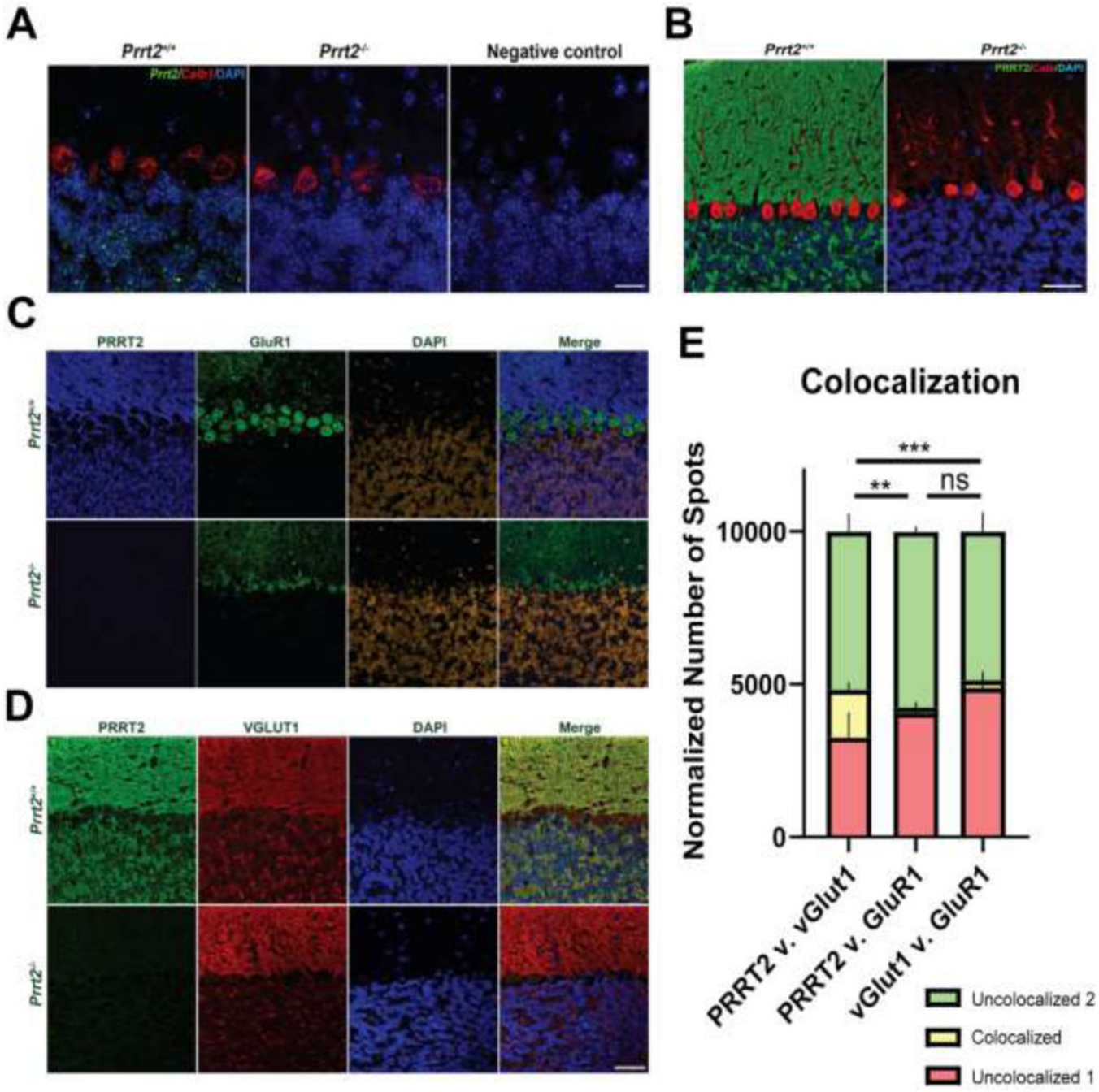


**Figure 4. Localization of PRRT2 within the cerebellar circuit**

**A.** *In-situ* hybridization of *Prrt2* transcripts (green) shows expression exclusively in the granule cell layer in *Prrt2*$^{+/+}$ mouse and absent in *Prrt2*$^{-/-}$ mouse cerebellar cortex. Scale bar = 20 μm. **B.** Fluorescent immunohistochemistry visualization of PRRT2 protein (green) in the cerebellar cortex. Protein is localized to the granule cell and molecular layers, with no colocalization with the Purkinje cell label, calbindin (red). Scale bar = 50 μm. **C.** Staining of PRRT2 (orange), GluR1 (green), and DAPI (blue). Merged image shows minimal colocalization of GluR1 and PRRT2. Scale bar = 50 μm. **D.** Staining of PRRT2

(green), vGlut1 (red), and DAPI (blue) showing extensive colocalization of vGlut1 and PRRT2. Scale bar = 50 μm. **E.** Spot analysis quantification of normalized colocalized spot number (n = 3 mice; unpaired t-test; * = $P<0.05$, ** = $P<0.01$, *** = $P<0.001$; mean ± SD).

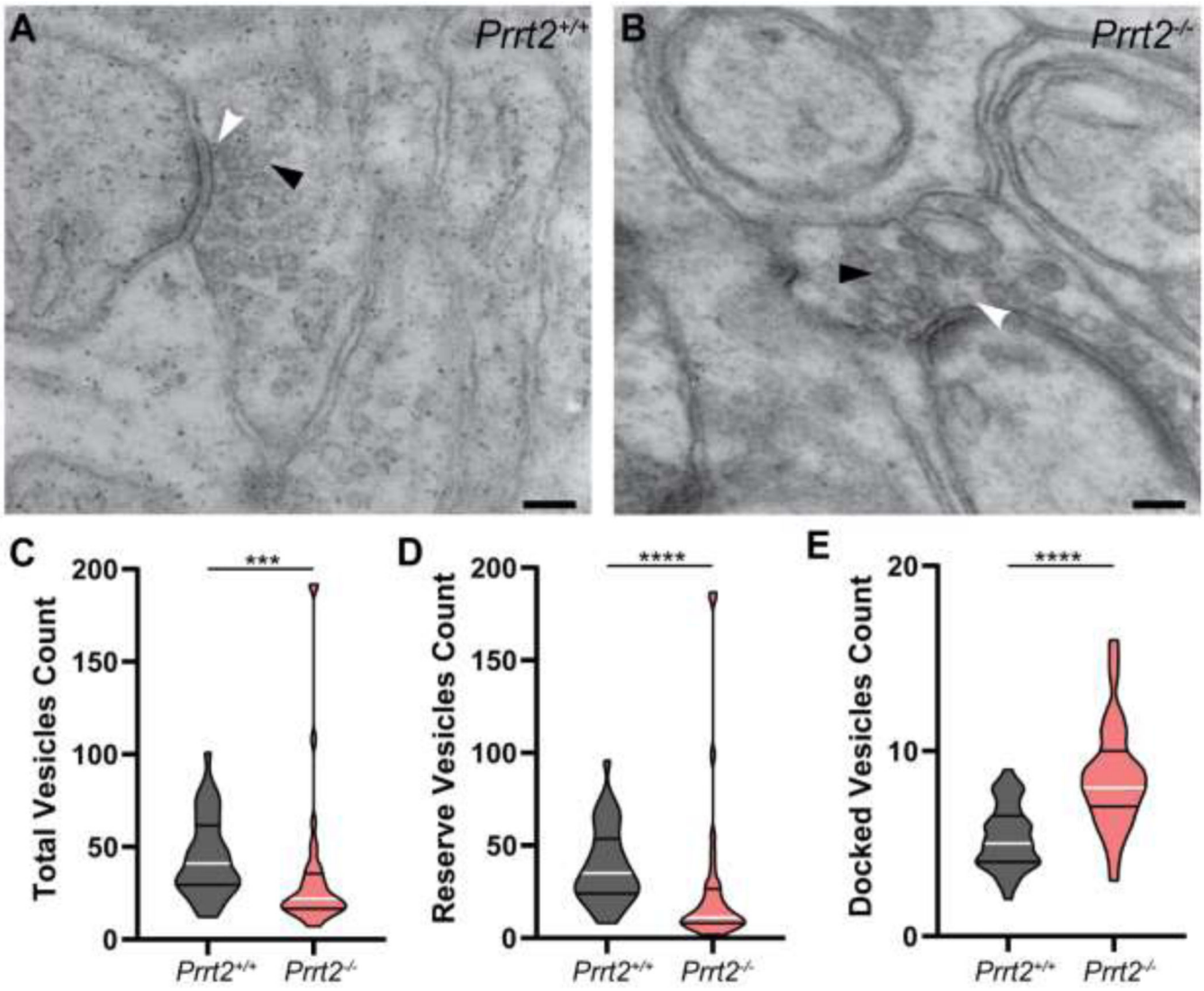


**Figure 5. Cerebellar cortex vesical localization in *Prrt2*$^{+/+}$ and *Prrt2*$^{-/-}$ mice.**

**A, B.** TEM images of vesicles in the molecular layer of cerebellar cortex of *Prrt2*$^{+/+}$ (left) and *Prrt2*$^{-/-}$ mice (right). White arrows denote docked vesicles, black arrows denote reserve vesicles. Scale bar = 100 nm **C-E.** Quantification of total vesicles, reserve vesicles, and docked vesicles in *Prrt2*$^{+/+}$ and *Prrt2*$^{-/-}$ mice (n = 37 synapses each; Mann-Whitney test; *** = $P$ <0.001, **** = $P$ <0.0001; horizontal white line is the median, black horizontal lines are the 25$^{th}$ and 75$^{th}$ percentiles).

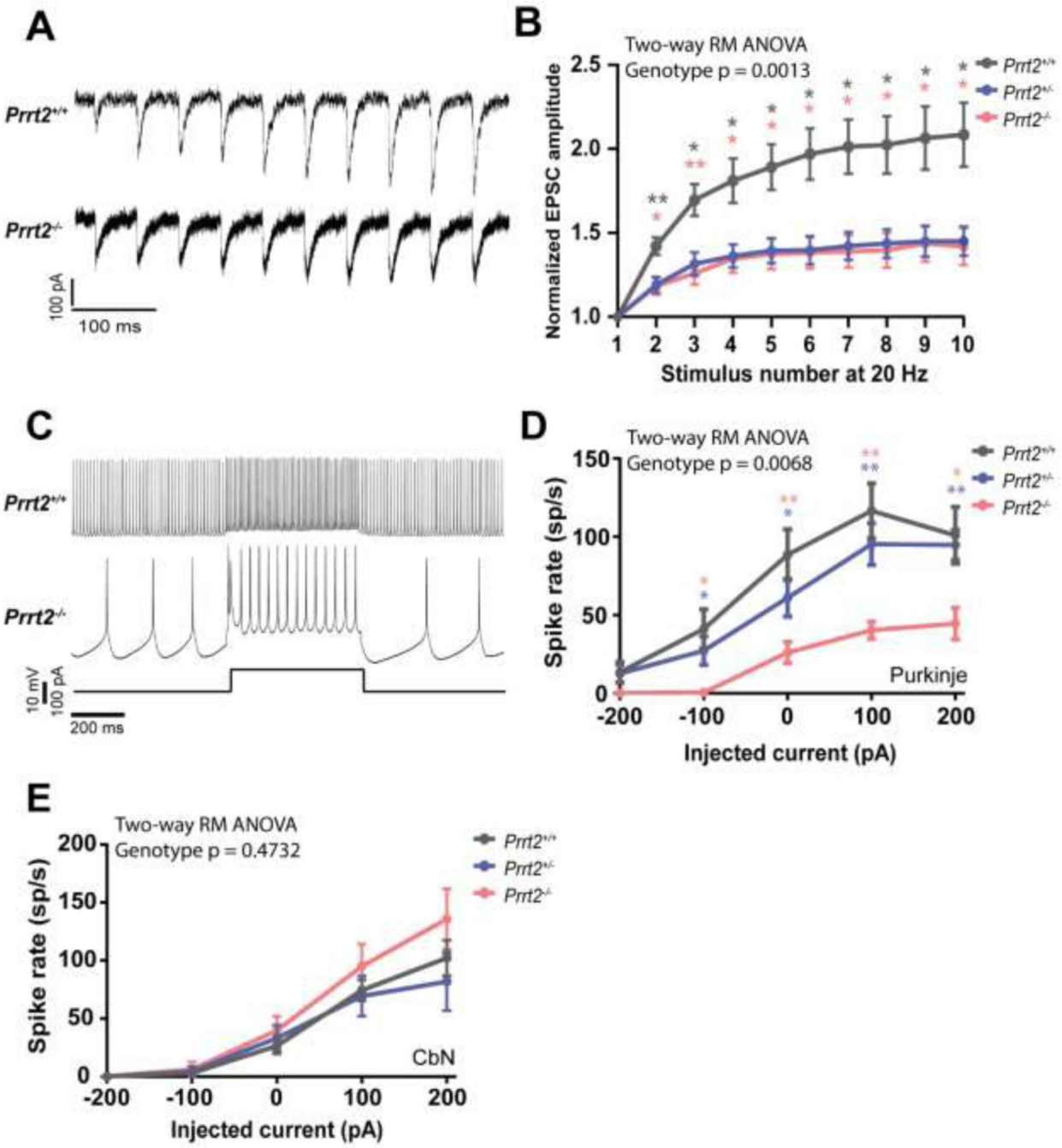


**Figure 6. *Prrt2* knockout alters Purkinje cell short-term facilitation and excitability.**

**A.** Examples of EPSCs in Purkinje cells evoked by 20-Hz parallel fiber stimulation in *Prrt2*$^{+/+}$ and *Prrt2*$^{-/-}$ mice. **B.** Amplitude of EPSCs evoked by successive stimulation of parallel fiber axons (two-way repeated measures ANOVA with Tukey's multiple comparison test; genotype: $F_{(2,29)} = 8.4$, $P = 0.0013$; asterisks indicate significance in Tukey's multiple comparison test; pink asterisks = *Prrt2*$^{+/+}$ vs *Prrt2*$^{-/-}$, grey asterisks = *Prrt2*$^{+/+}$ vs *Prrt2*$^{+/-}$; mean ± SEM). Values on the y axis are normalized to the amplitude of the first EPSC. **C.** Purkinje cell current clamp recordings showing response to 100-pA current injections

from *Prrt2*$^{+/+}$ and *Prrt2*$^{-/-}$ mice. **D.** Firing rate of Purkinje cells in response to injected current steps (two-way repeated measures ANOVA with Tukey's multiple comparison test; genotype: $F_{(2,50)} = 5.5$, $P = 0.0068$; asterisks indicate significance in Tukey's multiple comparison test; pink asterisks = *Prrt2*$^{+/+}$ vs *Prrt2*$^{-/-}$, blue asterisks = *Prrt2*$^{+/-}$ vs *Prrt2*$^{-/-}$; mean ± SEM). **E.** Summary of spike responses to injected current steps of CbN cells in current clamp mode (two-way repeated measures ANOVA with Tukey's multiple comparison test; genotype: $F_{(2,27)} = 0.77$, $P = 0.47$; mean ± SEM). * = $P < 0.5$, ** = $P < 0.01$.